



Comparison of Two SRM with No Flux-Reversal in the Stator

ABDULATE AHMUDA MUSBAH ELGANAI

Dept. of Electrical and Electronics Engineering, University of Bani waleed

ABSTRACT: A comparison of two configurations of a novel two- phase switched reluctance machine (SRM) with no flux reversal in the stator iron is presented in this paper. Conventional SRMs have flux reversals that occur in sections of the yoke during commutation. The two novel SRMs compared in this paper have six stator poles. Each phase comprises of three poles separated by 120° . The two rotor configurations contain three poles and nine poles, respectively. The comparison includes inductance and torque profiles, self-starting capability and torque ripple, weight, radial forces, core losses and in addition the unique features of the flux-reversal-free-stator SRMs. The results provide an indication of which machine is best suited for a particular application. Data for the comparison is obtained from dynamic finite element simulations.

KEYWORDS: two phase switched reluctance machine (SRM), flux reversal in the stator, conventional two phase SRM.

I. INTRODUCTION

Switched reluctance machines (SRM) have gained considerable attention in the field of low cost variable speed motor drive applications like home appliances such as vacuum cleaners and washing machines. Their low manufacturing cost, simple magnetic structure, fault tolerance and broad choice of converters [1], [2] depending on the requirements of the application, have made them a viable option for applications previously using universal or other AC machines.

Acoustic noise generated during the operation of SRMs have hindered their wide spread application. Acoustic noise, its antecedents and methods to reduce it in SRMs have been studied and proposed extensively [1], [3], [4], [5]. A new type of SRM with low-noise characteristics is also presented in [6]. Radial and tangential forces, and eccentricities in the air gap in SRMs introduce vibrations and deformations in the stator and rotor poles, and yoke. When these vibrations correspond with the natural frequency of the SRM structure, undesirable audible noise is amplified.

In this paper, two configurations of a novel two-phase SRM [7] with no flux reversal in the stator iron for low-acoustic noise are contrasted. The chosen configurations are two from a variety of possible configurations of two phase flux-reversal- free-stator SRMs having six stator poles and rotor poles in multiples of three. The two configurations presented in this paper will have three and nine rotor poles. One phase of the novel SRM is comprised of three stator poles separated by 120° . One pole in a phase carries the entire flux in the amount of flux and serve as its return path. Therefore, only two-thirds of the stator yoke carries flux through it when a phase is excited and consequently, core losses are reduced. No flux reversal occurs in the stator even when both phases are simultaneously excited. Due to the unique structure of the novel SRMs, the forces in the air gap are distributed across three stator poles which are separated by 120° . This unique feature along with no flux-reversal in the stator mitigates radial forces and acoustic noise in the SRM due to the distribution of the normal forces across a greater number of phase shifted stator poles [8].

This paper is organized as follows: Section II presents the two configurations and contrasts them with a conventional two-phase SRM. Section III describes the basis for comparison of the two machines and Section IV presents the results of the comparison. Section V shows experimental correlation of the design of one machine configuration. Conclusions drawn from the comparison are presented in Section VI.

II. CONVENTIONAL AND TWO FLUX-REVERSAL-FREE-STATOR SRMS

A. Conventional two-phase SRM

In a conventional two phase SRM with four stator poles and two rotor poles (4/2), radial forces in the air gap are distributed around two stator poles that are diametrically opposite. In two-phase SRMs which differ in the number of stator and rotor poles, radial forces are distributed around pole pairs that are diametrically separated. Furthermore, flux-reversals occurs in sections of the stator yoke during operation. Fig. 1 shows the flux-paths of a conventional 4/2 SRM when the two phases are excited independently. The stator yoke section A_1B_1 and A_2B_2 experience flux-reversal during commutation.

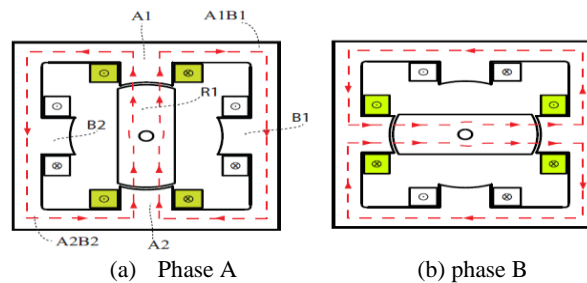


Fig. 1: Flux paths of a 4/2 SRM

B. 6/3 Flux-Reversal-Free-Stator SRM (Fig. 2)

The 6/3 SRM is comprised of six stator poles and three rotor poles. Fig. 2 shows the flux paths when each phase of the 6/3 SRM is excited independently. The flux direction in the stator

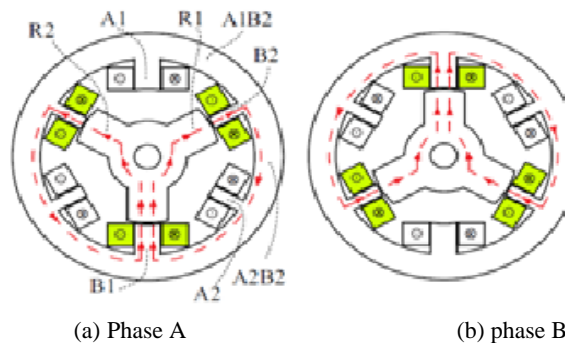


Fig. 2: Flux paths of a 6/3 SRM

poles and yoke sections are in the same direction regardless of which phase is excited. Furthermore, if both phases are excited simultaneously, due to the unidirectional flux path in the 6/3 SRM, the radial forces are distributed across all six stator poles. The flux distribution for a 6/3 SRM in different iron sections of the stator and rotor is shown in Fig. 3. The zero position in Fig. 3 corresponds to the rotor position shown in Fig. 2(a). The rotor is rotated counter-clockwise. The stroke angle of a conventional 6/3 SRM is 60° . The stroke period or angle is defined as the period or angle through which an SRM will generate positive torque in one phase. The flux distribution for the second phase can be derived by shifting the flux distribution waveforms by one stroke period (60°). A rotor pole and rotor yoke section experiences a flux reversal every 180° .

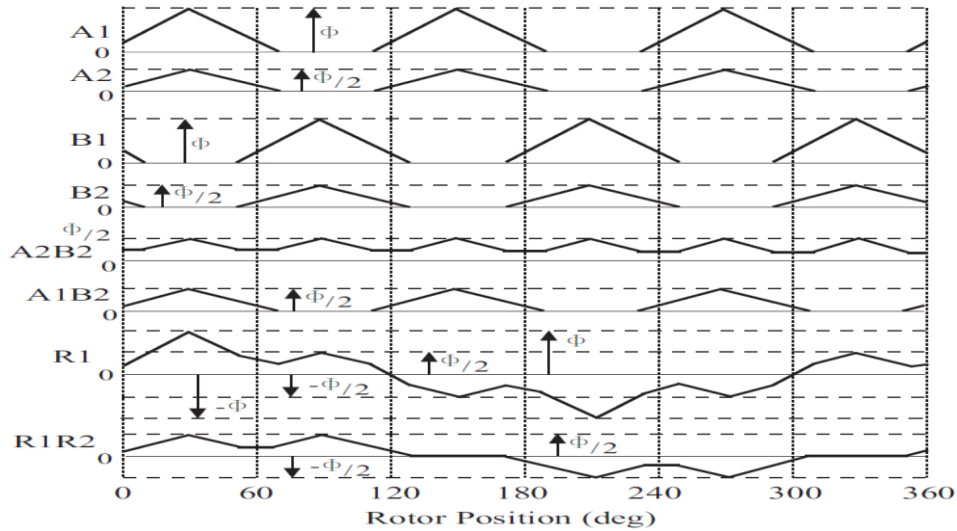


Fig. 3: Flux distribution for the 6/3 SRM iron sections

C. 6/9 Flux-Reversal-Free-Stator SRM (Fig. 4)

The 6/9 two-phase SRM configuration is comprised of six stator poles and nine rotor poles. The stroke angle of a conventional 6/9 SRM is 20°. The flux distribution of the SRM is shown in Fig. 5. Rotor poles and the rotor yoke experience a flux reversal every 180°.

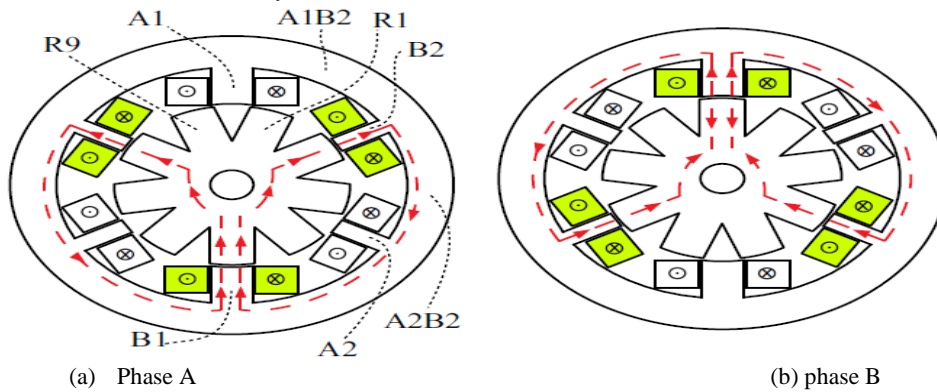


Fig. 4: Flux paths of a 6/9 SRM

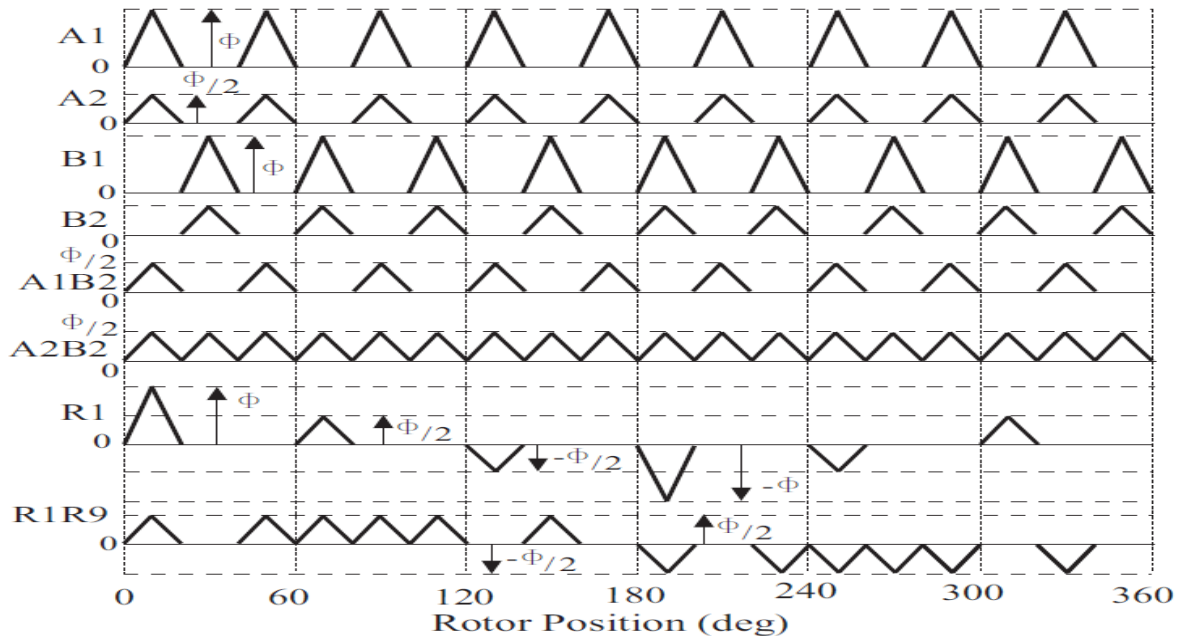


Fig. 5: Flux distribution for the 6/9 SRM iron sections

III. BASIS FOR COMPARISON

Several parameters and design criteria are applied to the design of the two machines. These parameters are:

- self-starting capability is incorporated into both SRMs to reduce cost and increase efficiency.
- the nominal operating voltage is 325 V (DC)
- minimum radial air gap length between the stator and rotor is set to 0.3 mm.
- M-19 steel is used for stator and rotor laminations.
- shaft diameter is same for both machines.
- rated torque of the SRMs is 3.75 N-m.
- asymmetric rotor pole faces are utilized in the design of the SRMs in order to facilitate torque profiling for self- starting and torque ripple reduction.
- stator frame used in designing both SRMs are same, hence the outer diameter of both machines is limited. operating speed of both machines is 1800rpm.

Finite element software, An soft Maxwell, is used to verify the designs and compare the two machines.

IV. RESULTS OF THE COMPARISON

A. SRM Dimensions

The 6/3 SRM was designed first and provided a benchmark for designing the 6/9 SRM. Once the 6/9 SRM lamination shape was optimized for torque production, the current ratings of the two machines were chosen to be the same leading to a lesser weight of the 6/9 SRM and hence a lower cost machine. The rated current for both machines is 10A. The 6/3 SRM has a heavier stator, rotor and windings when compared to the 6/9 SRM. The rotational inertia of the 6/3 rotor is approximately 3.5 times greater than the 6/9 rotor. This is due to the lower volume and weight of the rotor is which greatly affected by stack length. The 6/9 SRM has 30% less stack height than the 6/3 SRM. Keeping the stack length of both machines equal would result in a 15% lower rated current in the 6/9 SRM for the same operating conditions. Depending on the application requirements, a lower rated current may be more important than a lower machine weight. For the purpose of this comparison, the rated current of both SRMs are taken to be the same. The dimensions of the SR machines designed for the comparison are summarized in Table I.

TABLE I: Dimensions of the designed SRMs

	6/3 SRM	6/9 SRM
Air gap radius(mm)	43.7	43.7
Stator outer diameter (mm)	82	82
Main pole Arc	37 ⁰	21 ⁰
Auxiliary pole Arc	22 ⁰	16 ⁰
Rotor pole Arc	72 ⁰	21 ⁰
Stack length (mm)	85	60
Rotor mass (kg)	2.74	1.91
Stator mass (kg)	6.55	4.01
Rotational inertia (kg-m ²)	1.44*10 ⁻⁴	4.04*10 ⁻⁵
Winding turns per pole	110	110
Winding mass (kg)	1.39	1.07

B. Inductance Profile

Static inductance profiles of the 6/3 and 6/9 SRMs for various phase currents are shown in Fig. 6. The positive inductance slope region of the 6/3 SRM is approximately 75° which is greater than its conventional stroke angle (60°) resulting in an overlap between the positive inductance slopes of the two phases. The rotor poles of the 6/3 and 6/9 SRMs have non-uniform pole faces and wide pole arcs in order to maximize the positive inductance slope region. The positive inductance slope region is approximately 2° greater than the conventional stroke angle of 20° in the 6/9 SRM. An overlap in the rising inductance regions between the two phases also facilitates unidirectional self-starting at any rotor position. This feature can be seen in the torque profiles of the two machines which is shown in the following section. The lesser rotor pole pitch of the 6/9 SRM is unfavorable towards increasing the positive inductance slope region. Pole pitch is defined as the angle between the centers of two adjacent rotor poles.

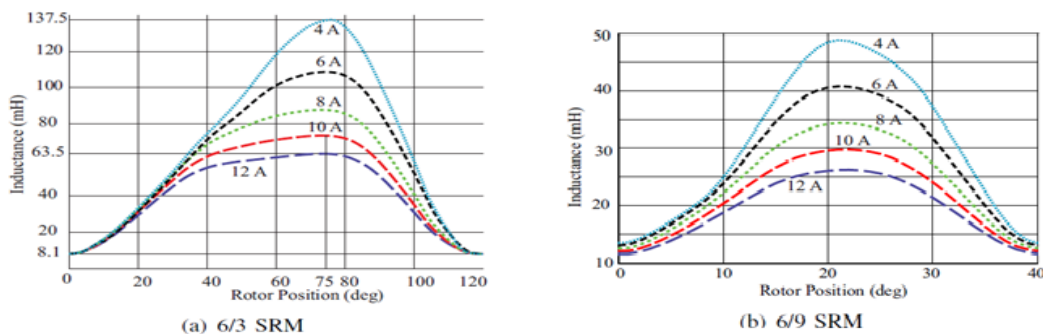


Fig. 6: Static inductance profiles of both SRMs for various currents

C. Torque Profiles

The overlap in the positive inductance slope between the two phases of both SRMs results in an overlap in the positive torque generated by each phase. Fig. 7 shows the positive torque profiles of the 6/3 and 6/9 SRMs. This

overlap allows for positive torque generation at all rotor positions. Hence self starting without external parking mechanisms for unidirectional rotation is achieved for both SRMs. The magnitude of the net torque generated by both phases in the overlapping region of the 6/3 SRM is greater than that of the 6/9 SRM. The lower rotational inertia of the rotor in the 6/9 SRM lends itself to a lesser amount of torque that is required to start the SRM from standstill. There is a 20% overlap between the torque generated by both phases of the 6/3 SRM and approximately 10% overlap in the 6/9 SRM. The larger rotor pole pitch of the 6/3 SRM allows greater flexibility in shaping the rotor pole to distribute torque over a wider stroke angle without sacrificing power density. Increasing the rotor pole arc in the 6/9 SRM by 4° resulted in a 21% drop in average static torque. The average torque with respect to phase currents is shown in Table II.

TABLE II: Comparison of the average static torque in the two SRMs

current	6/3 SRM	6/9 SRM
4	0.8	0.8
6	1.7	1.7
8	2.6	2.7
10	3.5	3.7
12	4.5	4.7

Fig. 8 shows the torque ripple in the SRMs during dynamic simulation of both SRMs at 1800 rpm. The asymmetric converter is used to drive the two SRMs. The 6/3 and 6/9 SRMs have advanced excitation angles that are 6° and 1.5°, respectively and advanced commutation angles which are 15° and 3°, respectively. The 6/9 SRM has a greater torque ripple than the 6/3 SRM with a rated load of 3.75 N-m on both machines. The peak-to-peak torque ripple is 5.1 N-m for the 6/3 SRM and approximately 7 N-m for the 6/9 SRM. Fig. 9 shows the normalized power spectral density of the electromagnetic torque shown in Fig 8. The 6/3 SRM has a phase switching frequency of 90 Hz at 1800rpm. The first and second harmonics are the most dominant frequencies in the electromagnetic torque for the 6/3 SRM because of two phases. The 6/9 SRM has a phase switching frequency of 270 Hz at 1800 rpm and its torque shows second harmonic to be most dominant frequency because of two phases. When these torque harmonics correspond to a vibration mode frequency of the stator, undesirable audible noise is amplified.

D. Radial Forces in the Air Gap

Radial and tangential forces in SRMs play a major role in generating undesirable acoustic noise. Majority of the radial forces are concentrated in the regions around the excited stator poles. Instantaneous forces in the air gap are estimated by evaluating the ‘Maxwell Stress Tensor’ directly in FE software by using the following the equation [9],

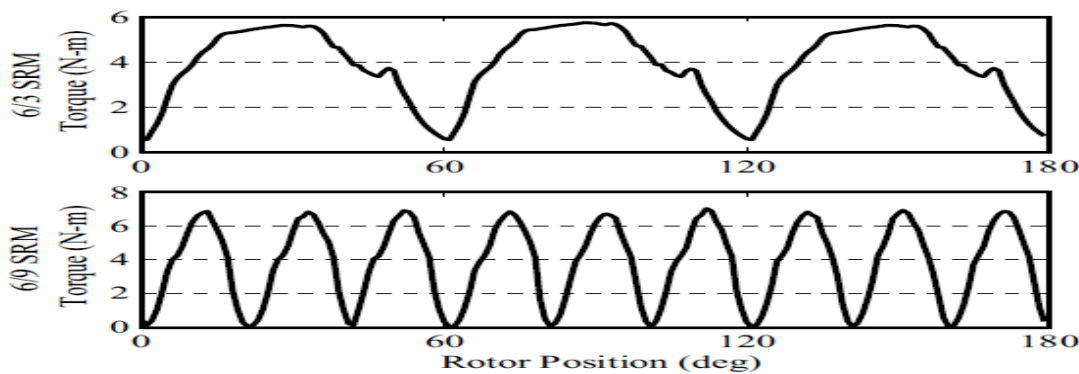


Fig. 8: Simulated electromagnetic torque at 1800 rpm with 3.75 N-m load

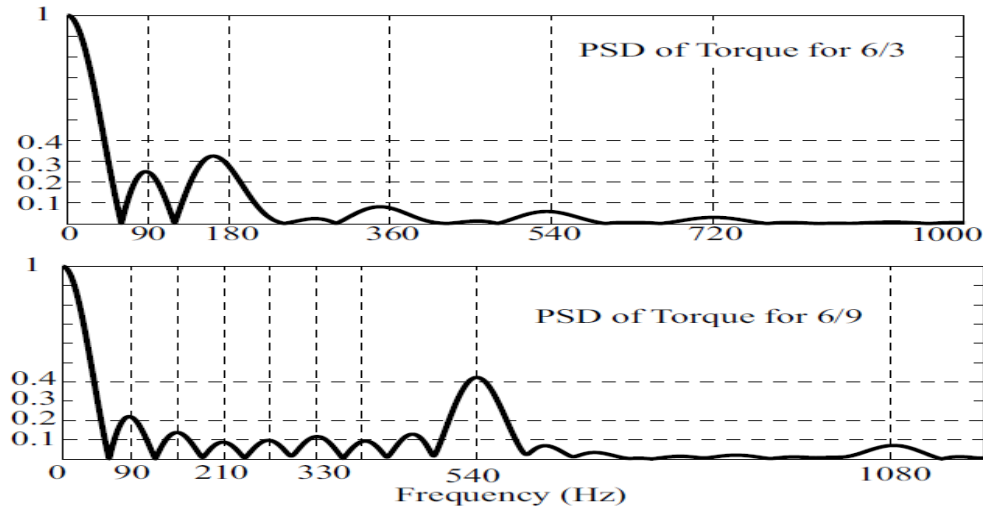


Fig. 9: Normalized power spectral density of the electromagnetic torque for both SRMs at 1800rpm

$$f = \int Real |(\vec{B} \cdot \vec{n})\vec{H} - 0.5(\vec{B} \cdot \vec{H})\vec{n}|dV \quad (1)$$

where \vec{B} is the flux density vector, \vec{H} is the magnetic field intensity vector and \vec{n} is a unit normal vector to a circle in the air gap on which the radial forces are estimated. Figs. 10(a) and 10(b) show the instantaneous force density (N/m) on the periphery of the air gap between the stator and rotor for both 6/3 and 6/9 SRMs. The axes used in the force density figure shown in Fig. 10 are described in Fig. 11 for a 6/9 SRM. ‘ Φ ’ is the absolute air gap position and θ is the rotor position. ‘ θ ’ begins from the unaligned position of the rotor and ends at the next unaligned position. The current is held at 10A for both machines. Force density for the auxiliary stator poles is less than that of the main pole since each pole carries half the flux of the main pole and has a smaller pole arc. Figs.12(a) and 12(b) show average radial force around the three excited stator poles which is calculated from the force densities around each stator pole for each rotor position shown in Fig. 10. Fig. 13 shows the resultant force magnitude and angle of the vector sum of the radial forces around the three excited stator poles evaluated by the following expression,

$$|F_r|\angle\delta = |F_{A1}|\angle 0 + |F_{A2}|\angle \frac{2\pi}{3} + |F_{A3}|\angle -\frac{2\pi}{3} \quad (2)$$

where A1 is the main pole of phase A, and A2 and A3 are the auxiliary poles of the same phase. The vector sum of the radial forces shows the unbalanced radial forces in the flux-reversal-free-stator SRMs. The peak magnitude of the radial force resultant in the 6/3 SRM is three times greater than that of the 6/9 SRM.

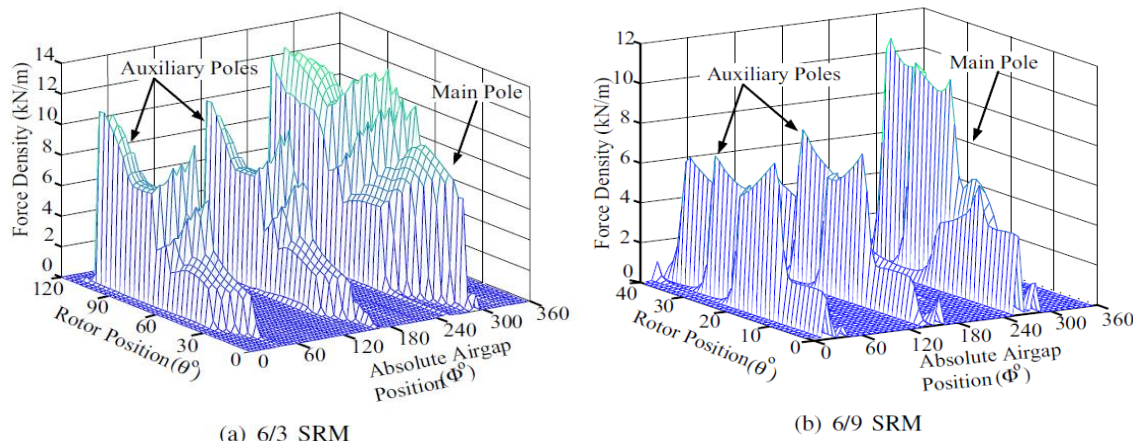


Fig. 10: Force density with respect to absolute air gap position and rotor position for the 6/3 and 6/9 SRMs

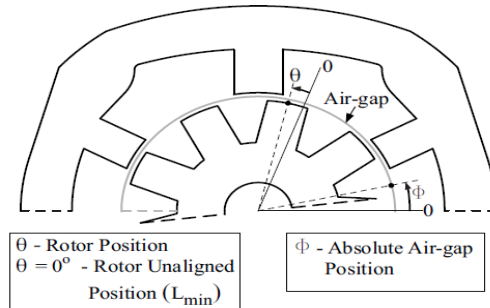
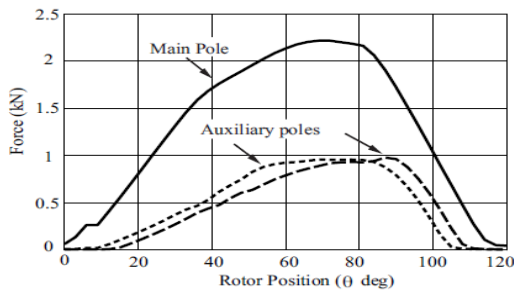
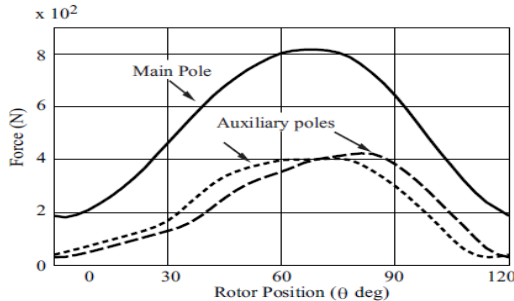


Fig. 11: Legend for radial force density result shown in Fig.10



(a) 6/3 SRM



(b) 6/9 SRM

Fig. 12: Radial forces around each excited pole for both SRMs

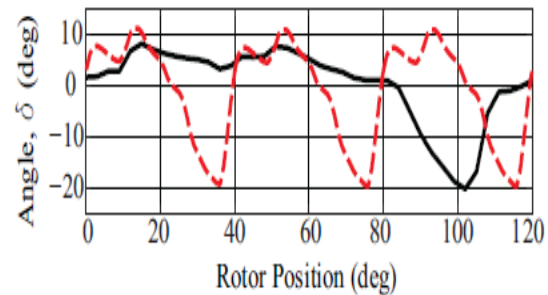
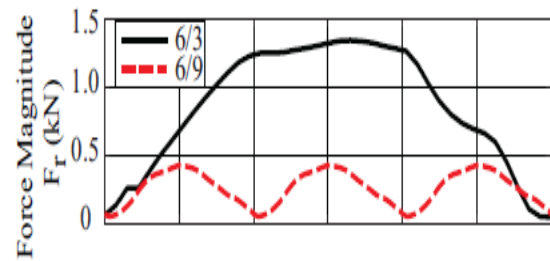


Fig. 13: Instantaneous radial force resultant for both SRMs

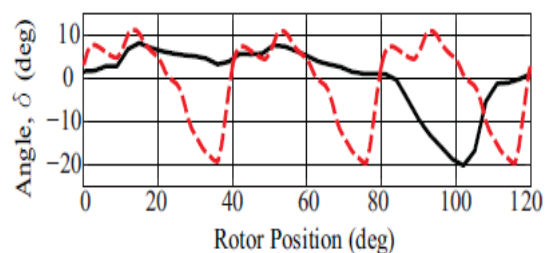
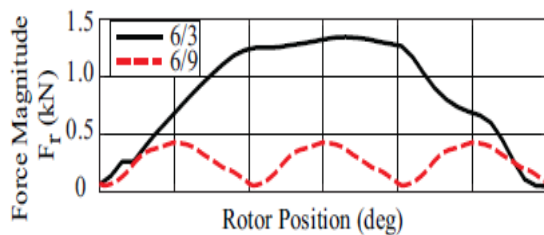


Fig. 13: Instantaneous radial force resultant for both SRMs

E. Core Losses

Core losses are proportional to the frequency of the flux, the magnitude of the flux density and weight of material traversed by the flux. A unique feature of the 6/3 and 6/9 SRMs is that the stator and rotor pole combinations give two-third utilization of the stator and rotor back irons at any time of its operation thus resulting in smaller flux paths. In conventional SRMs flux traverses the entire stator yoke resulting in greater core losses. Smaller flux paths require smaller magneto motive force (mmf) leading to higher efficiency during operation.

Dynamic FE simulations of the SRMs at 1800 rpm with asymmetric converter are performed and the average flux densities for each stator and rotor section are calculated for every degree of rotation. The average flux densities

are normalized and are approximated using fourth-order polynomial equations. Eddy losses can then be directly estimated using equations described in [10], [11]. Hysteresis losses in the stators of both SRMs are reduced due to unipolar flux waveforms. The eddy and hysteresis losses for both machines are given in Table III.

TABLE III: Core-loss estimate for the two machines (Watts)

	6/3 SRM		6/9 SRM	
	Eddy	Hysteresis	Eddy	Hysteresis
Stator	6.0	7.6	14.5	11.1
Rotor	3.3	4.9	6.3	5.4
Total	22		38.3	

V. EXPERIMENTAL RESULTS

A prototype of the designed 6/3 SRM was available for correlation of the inductance profile from FE simulations to verify the validity of the design of the SRMs. Fig. 14 shows the measured and FEA inductance of the 6/3 SRM for three currents. There is good correlation of the inductance from FEA and measured values at high saliency ratios and small error at high currents which is acceptable given error in the material data and eccentricities in the air gap of the prototype machine. A 6/9 SRM was not available for experimental correlation at this time.

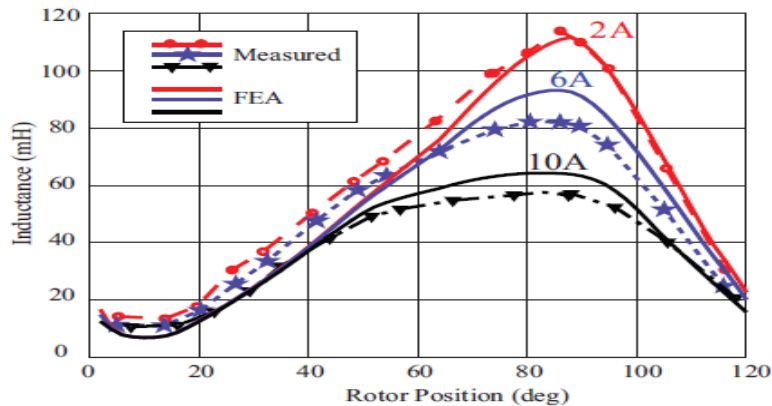


Fig. 14: Experimentally measured inductance correlated with FEA inductance of the designed 6/3 SRM

VI. CONCLUSIONS

This paper compared two SRM configurations with no flux-reversal in the stator. The following conclusions can be drawn from the analysis:

- 6/3 SRM is advantageous for torque profiling with asymmetric rotor pole faces without greatly sacrificing power density.
- 6/9 SRM has higher power density for the same operating conditions as the 6/3 SRM.
- Both SRMs are capable for self-starting from any position for unidirectional rotation.
- Radial forces in 6/9 SRM are 60% lower than the 6/3 SRM.
- Torque ripple with the 6/3 SRM is 27% lower than the 6/9 SRM.
- Both SRMs have no flux-reversal and core-losses are reduced as a result.
- Core-losses in the 6/3 SRM are much smaller than 6/9 SRM.



ISSN: 2350-0328

International Journal of Advanced Research in Science, Engineering and Technology

Vol. 8, Issue 2 , February 2021

REFERENCES

- [1] R. Krishnan, Switched Reluctance Motor Drives: Modeling, Simulation, Analysis, Design, and Applications. CRC Press LLC., June 2001.
- [2] M. Barnes and C. Pollock, "Power electronic converters for switched reluctance drives," *IEEE Transactions on Power Electronics*, vol. 13, no. 6, pp. 1100–1111, Nov. 1998.
- [3] D. Cameron, J. Lang, and S. Umans, "The origin and reduction of acoustic noise in doubly salient variable-reluctance motors," *IEEE Transactions on Industry Applications*, vol. 28, no. 6, pp. 1250–1255, Nov.-Dec. 1992.
- [4] C.-Y. Wu and C. Pollock, "Analysis and reduction of vibration and acoustic noise in the switched reluctance drive," *IEEE Transactions on Industry Applications*, vol. 31, no. 1, pp. 91–98, Jan.-Feb. 1995.
- [5] M. Anwar, I. Husain, S. Mir, and T. Sebastian, "Evaluation of acoustic noise and mode frequencies with design variations of switched reluctance machines," *IEEE Transactions on Industry Applications*, vol. 39, no. 3, pp. 695–703, May-June 2003.
- [6] Abdulate A. M. Elganai "Study of Rotary-Linear Switched Reluctance Motor" *International Journal of Engineering Trends and Technology (IJETT)* - SSN: 2231-5381– Volume 31 No 3- pp 149-152 January 2016.
- [7] R. Krishnan and N. S. Lobo, "Apparatus and method that prevent flux reversal in the stator back material of a two-phase srm (tpsrm)," U.S. Patent 7,015,615, March 21, 2006.
- [8] S.-G. Oh and R. Krishnan, "Two phase srm with flux reversal free stator: Concept, analysis, design and experimental verification," Accepted for Publication in 41st IAS Annual Conference of the IEEE, 2006.
- [9] Ansoft Corporation, "Instantaneous forces on bus bars." Maxwell 3D Application Note.
- [10] Y. Hayashi and T. Miller, "A new approach to calculating core losses in the srm," *IEEE Transactions on Industry Application*, vol. 31, no. 5, pp. 1039–1046, Sept.-Oct. 1995.
- [11] P. Vijayraghavan, "Design of switched reluctance motors and development of a universal controller for switched reluctance and permanent magnet brushless dc motor drives," Ph.D. dissertation, Virginia Tech, 2001.
- [12] W. Pengov, J. Hendershot, and T. Miller, "A new low-noise two-phase switched reluctance motor," *IEEE International Conference on Electric Machines and Drives*, pp. 1281 – 1284, 2005.